

Supporting Information

“Understanding the Crucial Role of Local Crystal Order in Electrocatalytic Activity of Crystalline Manganese Oxide”

Jang Mee Lee,^a Sharad B. Patil,^a Bohyun Kang,^a Seul Lee,^a Min Gyu Kim,^b and Seong-Ju Hwang^{a,*}

^a Center for Hybrid Interfacial Chemical Structure (CICS), Department of Chemistry and Nanoscience, College of Natural Sciences, Ewha Womans University, Seoul 03760, Republic of Korea

^b Pohang Light Source, Pohang 37673, Republic of Korea

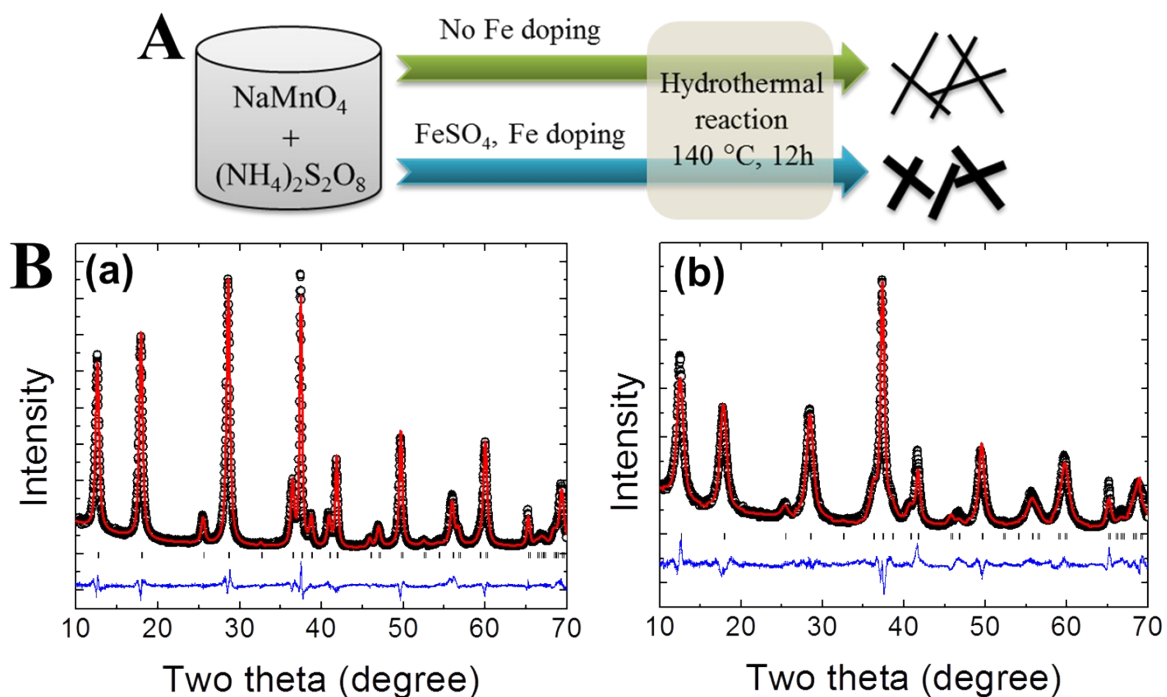


Fig. S1 (A) Schematic model for synthesis of Fe-substituted $\alpha\text{-Mn}_{1-x}\text{Fe}_x\text{O}_2$ nanowire. (B) Powder X-ray diffraction (XRD) patterns with Rietveld fits for (a) unsubstituted **FMO0** and (b) Fe-substituted **FMO10**. Experimental data, calculated profiles, allowed Bragg reflection positions, and difference curve are presented with black circles, red line, vertical bars, and blue line, respectively.

: As illustrated in Fig. S1A, Fe-substituted $\alpha\text{-Mn}_{1-x}\text{Fe}_x\text{O}_2$ nanowires are synthesized by hydrothermal reaction of the ion-adducts of MnO_4^- - Fe^{2+} . As presented in the Rietveld refinement results of Fig. S1B, all the powder XRD peaks of the present $\alpha\text{-Mn}_{1-x}\text{Fe}_x\text{O}_2$ ($x = 0$ and 0.1) materials are well-reproduced with tetragonal ($I4/m$) $\alpha\text{-MnO}_2$ structure composed of corner- and edge-shared MnO_6 octahedra with 2×2 tunnels,^{1,2} confirming the successful substitution of Mn with Fe without the formation of impurity phase.

	FMO0	FMO10
<i>a</i> (Å)	9.84	9.89
<i>b</i> (Å)	9.84	9.89
<i>c</i> (Å)	2.85	2.86
cell vol.	276	280
R _{wp} (%)	6.66	9.21
R _p (%)	5.15	7.03
reduced χ^2	3.60	6.33

Table S1. Crystallographic data and fitting details of Rietveld refinements.

: The larger lattice parameters and volumes are estimated from the XRD patterns measured in Fourier transform (FT) mode for the unsubstituted **FMO0** and its Fe-substituted **FMO10**.

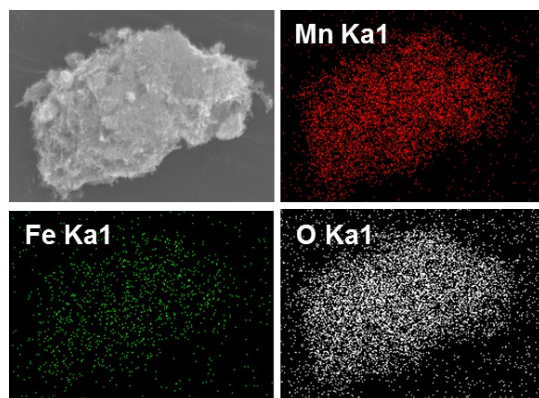


Fig. S2 Energy dispersive spectrometry (EDS)–elemental maps of **FMO10**.

: As illustrated in Fig. S2, homogeneous Fe substitution in the **FMO10** nanowire is cross-confirmed by EDS–elemental mapping analysis showing the uniform distributions of Mn, Fe, and O elements.

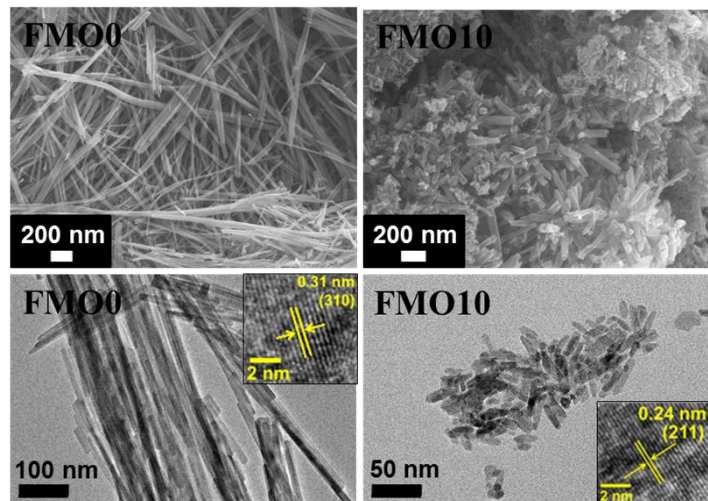


Fig. S3 (Top) Field emission-scanning electron microscopy (FE-SEM) images, and (bottom) high resolution-transmission electron microscopy (HR-TEM) images of unsubstituted **FMO0** and Fe-substituted **FMO10**.

: The inset of HR-TEM graph shows the lattice fringe of each material. In the FE-SEM images of Fig. S3A, all the present $\alpha\text{-Mn}_{1-x}\text{Fe}_x\text{O}_2$ ($x = 0$ and 0.1) materials display 1D nanostructure morphology. In comparison with the **FMO0**, the **FMO10** exhibits shorter length of several hundreds of nanometer, reflecting the remarkable frustration of the 1D crystal growth of $\alpha\text{-MnO}_2$ nanowire caused by the substitution of Fe ion. The morphological evolutions of $\alpha\text{-MnO}_2$ nanowire upon the Fe substitution are further evidenced by HR-TEM, see Fig. S3B. The observation of clear lattice fringes corresponding to the (301), (200), and (220) planes of $\alpha\text{-MnO}_2$ structure verifies the maintenance of tetragonal $\alpha\text{-MnO}_2$ lattice in the present materials.

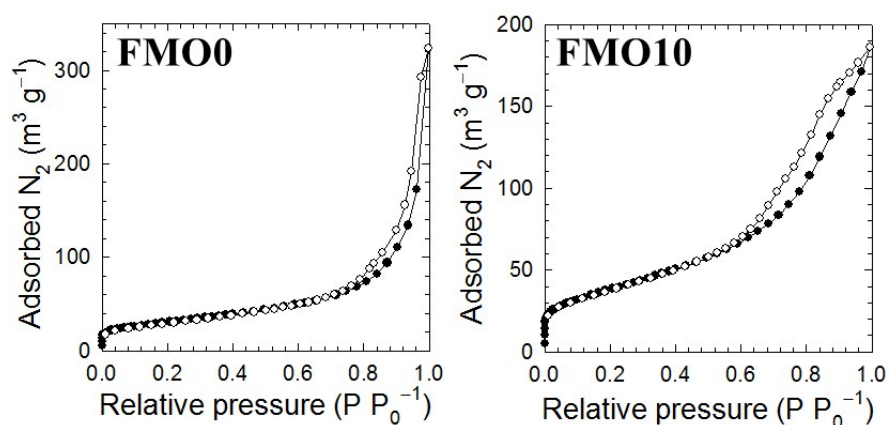


Fig. S4 N_2 adsorption–desorption isotherms of **FMO0** and **FMO10**. The close and open symbols represent the adsorption and desorption data, respectively.

: As shown in N_2 adsorption–desorption isotherms of Fig. S4, all the present materials commonly exhibit distinct hysteresis at $p/p_0 > 0.5$, indicating the presence of mesopores originating from the stacking structure of 1D nanowires. Based on Brunauer–Emmett–Teller (BET) equation, the surface area of the Fe-substituted material is determined as $112 \text{ m}^2 \text{ g}^{-1}$ for **FMO10**, which is greater than that of unsubstituted **FMO0** ($64 \text{ m}^2 \text{ g}^{-1}$). This result clearly demonstrates the beneficial role of Fe substitution in expanding the surface area of $\alpha\text{-MnO}_2$ nanowire.

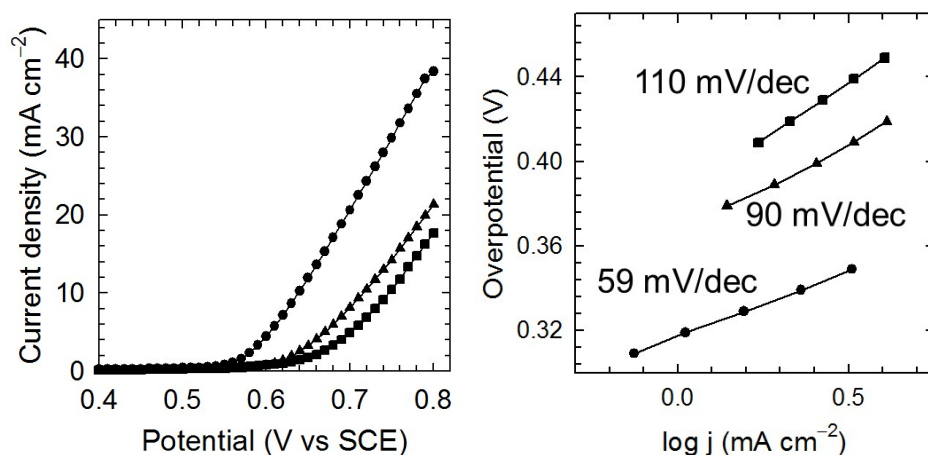


Fig. S5 (Left) Linear sweep voltammetry (LSV) curves and (right) Tafel slope of **FMO0** (squares), **FMO10** (circles), and the physical mixture of α -MnO₂ and Fe₂O₃ (triangles) with the same Fe/Mn ratio as that of **FMO10** measured in an anodic direction.

: As plotted in Fig. S5, the physical mixture of α -MnO₂ and Fe₂O₃ shows much poorer electrocatalyst performance with smaller current density, higher overpotential, and higher Tafel slope than does the Fe-substituted **FMO10**, highlighting the negligible contribution of Fe ion as an OER active site. This result clearly demonstrates that the enhancement of OER activity upon the Fe substitution is attributable not to the role of substituted Fe ion as an electrocatalytically active site but to the modification of α -MnO₂ lattice caused by the partial replacement of Mn with Fe.

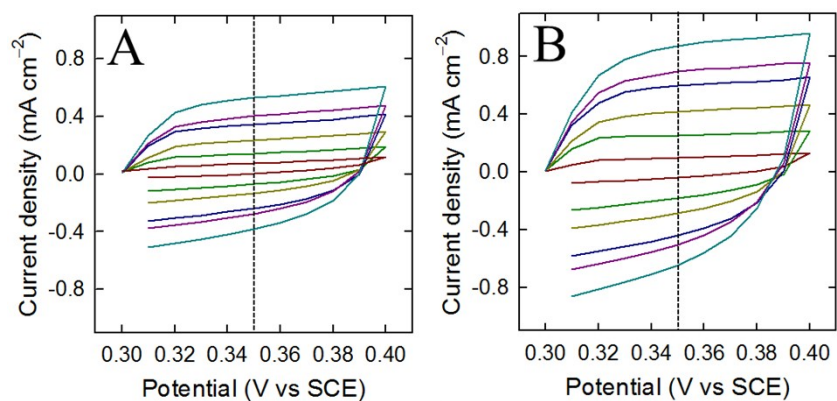


Fig. S6 Cyclic voltammetry curves of (A) **FMO0** and (B) **FMO10** measured in 0.1 M KOH with different scan rates of 20, 40, 60, 80, 100, and 120 mV s⁻¹.

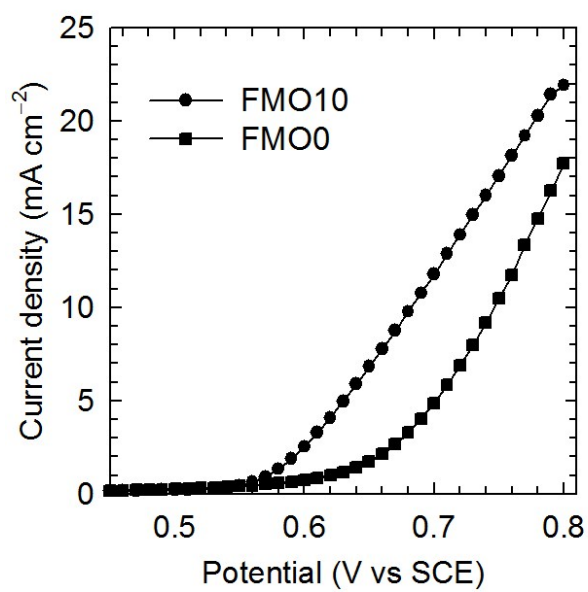


Fig. S7 LSV curve normalized by the ECSA value for the **FMO0** and **FMO10** materials.

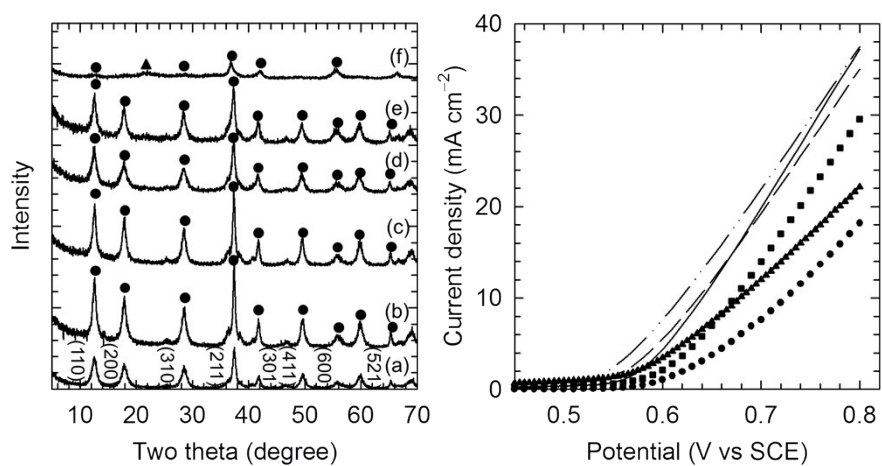


Fig. S8 (Left) XRD patterns and (right) LSV curves for $\alpha\text{-Mn}_{1-x}\text{Fe}_x\text{O}_2$ with $x = 0$ (a, circles), 0.05 (b, squares), 0.1 (c, solid), 0.2 (d, dash), 0.3 (e, dash-dot-dot-dash), and 0.35 (f, triangles).

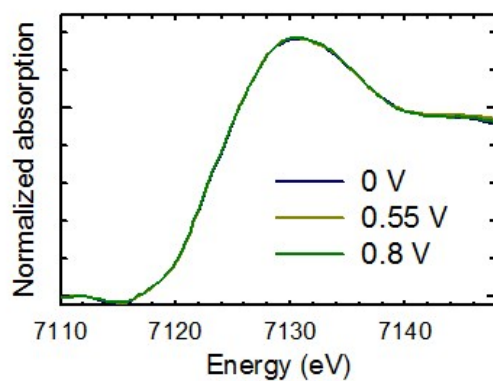


Fig. S9 *In-situ* Fe K-edge XANES spectra of **FMO10** measured at the various potentials of 0, 0.55, and 0.8 V. The present spectra were obtained as fluorescence mode.

: As plotted in Fig. S7, applying oxidative potentials to Fe-substituted **FMO10** causes negligible spectral change in Fe K-edge XANES spectra.

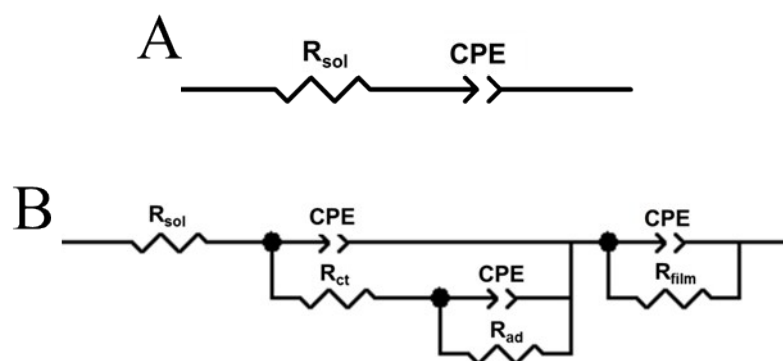


Fig. S10 Equivalent circuits for the simulation of the EIS data measured at (A) 0, and 0.3 V, and (B) 0.55, 0.7, and 0.8 V.

	R_{sol}	R_{ct}	R_{ad}	R_{film}
FMO0 at 0 V	114.4			
FMO0 at 0.3 V	98.89			
FMO0 at 0.55 V	109.5	2757	816.8	1598
FMO0 at 0.7 V	70.86	29.46	55.62	24.75
FMO0 at 0.8 V	70.4	26.88	4.15	25.04
FMO10 at 0 V	93.66			
FMO10 at 0.3 V	67.69			
FMO10 at 0.55 V	83.21	8.76	172.5	45.71
FMO10 at 0.7 V	67.46	5.91	6.09	22.62
FMO10 at 0.8 V	73.23	0.98	2.79	7.43

Table S2. Simulated parameters for the electrochemical impedance spectroscopy (EIS) data measured at the various potentials of 0, 0.3, 0.55, 0.7, and 0.8 V. R_{sol} , R_{ct} , R_{ad} , and R_{film} represent solution resistance, charge transfer resistance, adsorption resistance, and film resistance, respectively.

Reference

- 1 S. L. Suib, *Acc. Chem. Res.*, 2008, **41**, 479–487.
- 2 S. L. Suib, *J. Mater. Chem.*, 2008, **18**, 1623–1631.